ACI MATERIALS JOURNAL TECHNICAL PAPER

Title No. 114-M52

Effect of Multiaxial Stresses on Alkali-Silica Reaction Damage of Concrete

by Bishnu Prasad Gautam, Daman K. Panesar, Shamim A. Sheikh, and Frank J. Vecchio

Alkali-silica reaction (ASR) causes expansion, cracking, and degradation of the mechanical properties of concrete. While ASR performance of unrestrained concrete specimens is relatively well understood, the ASR performance of concrete structures is complicated by co-acting stresses. This paper investigates the influence of sustained multiaxial stresses on the response of concrete undergoing ASR. Reactive concrete cube specimens (with three replicates) were subjected to different stress states, from no-stress to triaxial stress, and were subjected to accelerated curing until the exhaustion of expansion potential. The specimens were periodically core-drilled and the cores were tested for compressive strength and modulus of elasticity. Stress state influenced the degradation of mechanical properties and ASR-affected concrete behaved as an orthotropic material. ASR cracking was portrayed along three mutually perpendicular planes of multiaxially loaded concrete by performing damage rating index analysis. Surface cracking was also monitored. Triaxial confinement contributed to having reduced volumetric expansion and less cracking.

Keywords: alkali-silica reaction; damage rating index; expansion; mechanical properties; multiaxial stresses.

INTRODUCTION

Alkali-silica reaction (ASR) is a serious deterioration problem in many concrete structures around the world.[1] The reaction causes expansion, cracking, and degradation of mechanical properties of concrete. Although generally it is now possible to construct new structures safe against ASR, the greatest challenge remains to ensure the performance of existing ASR-affected structures by assessing ASR damage.

Damage assessment of ASR-affected concrete usually relies on measuring expansion, monitoring cracking, and testing mechanical properties. Measurements on unrestrained specimens have established expansion as a characteristic of ASR. However, concrete in structures is often subjected to stresses in one or multiple directions and, hence, expansion measured on unrestrained laboratory specimens does not appropriately reflect concrete behavior in the structures. ASR expansion is the external manifestation of the damage occurring inside the concrete and is thus largely influenced by the stress state of concrete.[2-5] Apart from the expansion measurement, an understanding of the cracking and the degradation of mechanical properties is essential in evaluating the performance of ASR-affected concrete structures.

Cracks have been monitored as a means of assessing damage of existing concrete structures. Surface cracks have been mapped to assess the ASR damage experienced by concrete structures, sometimes in terms of a "cracking index".[6,7] However, the cracking index method involves monitoring cracks along the four sides and two diagonals of a square area on a concrete surface, and does not differentiate the cracks by their orientation, which can be influenced by the stress state of concrete.[8] Another method to assess the damage due to ASR by monitoring cracking is the damage rating index (DRI). The DRI method was developed in the 1990s as a means of quantitatively assessing the damage of the concrete microstructure due to ASR. The DRI is rooted on cracking that is characteristic of ASR damage and accounts for seven damage features. For concrete structures, the DRI method can be applied to concrete samples taken from the structures even without a reference measurement. While the DRI method has been extensively applied to laboratory concrete specimens[9-11] and to the cores from existing structures,[12] the influence of stress state on damage has not been studied. Grattan-Bellew[12] observed widely varying surface cracking and DRI values of cores from different parts of an ASR-affected dam and viewed the variation as "difficult to explain." While variation in the reactivity of aggregate and moisture content were indicated as possible causes, it is possible that the influence of stress state might also have a role in those variations. Stress state may cause spatial and directional variations in the cracking and the DRI values of concrete in the ASR-affected structures.

Testing mechanical properties is another method of assessing ASR damage. Many studies have reported on the degradation of mechanical properties of concrete due to ASR.[13-17] However, such studies mostly test unrestrained specimens that do not truly represent the ASR damage of structural concrete having a variety of stresses, as indicated by Giaccio et al.[18] Degradation of mechanical properties in the context of concrete structures is sometimes assessed by testing cores taken from ASR-affected concrete structures.[12,19,20] Such tests have been the basis of the "stiffness damage test" that was proposed as a tool to evaluate the ASR damage.[21,22] However, the focus of the studies was to relate stiffness damage test results to the ASR expansion. Even though testing of over 1000 cores from several ASR-affected structures was reported,[23] the influence of stress state on the evolution and consequence of ASR has been inadequately acknowledged. Because ASR damage can be influenced by the concrete's stress state, the information

ACI Materials Journal, V. 114, No. 4, July-August 2017.
MS No. M-2016-135.R1, doi: 10.14359/51689617, received September 28, 2016,

Table 1—Chemical composition of cement

Constituents	LOI	SiO_2	Al_2O_3	Fe_2O_3	CaO	MgO	SO_3	Total alkali (Na_2O_{eq})	Free lime	Insoluble residue
Percentage (by mass)	2.27	19.25	5.33	2.41	62.78	2.36	4.01	0.99	1.29	0.52

Table 2—Seven stress states in concrete cube specimens

Stress state	Designation	f_x	f_y	f_z	Number of cube specimens
		MPa (psi)			
No-stress	n (0, 0, 0)	0 (0)	0 (0)	0 (0)	3 + 1
Uniaxial	u (3.9, 0, 0)	3.9 (566)	0 (0)	0 (0)	3
	U (9.6, 0, 0)	9.6 (1392)	0 (0)	0 (0)	3
Biaxial	b (3.9, 3.9, 0)	3.9 (566)	3.9 (566)	0 (0)	3
	B (9.6, 3.9, 0)	9.6 (1392)	3.9 (566)	0 (0)	3
Triaxial	t (3.9, 3.9, 3.9)	3.9 (566)	3.9 (566)	3.9 (566)	3
	T (9.6, 3.9, 3.9)	9.6 (1392)	3.9 (566)	3.9 (566)	3

provided by two cores at the same location, but along two directions, represents two widely different scenarios. Large variations have been observed in the mechanical properties of cores from reinforced concrete members taken parallel and perpendicular to the longitudinal reinforcement.[19,24] The prestressing effect produced by the reinforcing steel due to the expansive pressure from ASR was basically attributed for such directional variations,[20,24] even though the strength of cores might have been influenced to some extent by the direction of cores relative to the direction of casting of concrete.[25] However, the stress level and its relationship to the degradation of mechanical properties of concrete due to ASR has not been explored. Because the effect of restraint is essentially through the prestressing stress it applies on concrete, a clear understanding of the effect of stress state on the degradation of mechanical properties of concrete due to ASR can help in reliably evaluating the performance of ASR-affected concrete structures.

This study is focused on the damage of ASR concrete subjected to multiaxial stresses. Twenty-one cube specimens with three replicates of seven stress states, from no-stress to triaxial stress, and an additional reference specimen were subjected to high-temperature (50 ± 0.5°C [122 ± 0.9°F]), high-humidity (>95% relative humidity) accelerated curing until the exhaustion of the expansion potential. The specimens were periodically measured for triaxial expansion from the day of demolding to the exhaustion of the reaction.[2] To further understand the evolution and consequences of ASR, the cube specimens were periodically core-drilled, and the cores were tested for compressive strength and modulus of elasticity. In addition, degradation of mechanical properties was studied through many companion cylinders. The cubes were analyzed for the DRI along three mutually perpendicular planes. This paper reports the results from such tests. Also reported is the surface cracking of cube specimens.

RESEARCH SIGNIFICANCE

ASR damage of concrete is a serious problem in existing structures. While concrete in structures is subjected to various stress states, the mechanism of ASR has been mostly investigated for unrestrained specimens. This study investigates the influence of uniaxial, biaxial, and triaxial stresses on the ASR-affected concrete by analyzing triaxial expansion, cracking along three planes, and degradation of the mechanical properties along stressed and unstressed directions. By integrating the understanding of triaxial expansion, cracking, and degradation of mechanical properties, this study is anticipated to expand the material level understanding of ASR to the structural response of ASR-affected concrete structures.

EXPERIMENTAL INVESTIGATION

Concrete ingredients and mixture design

The concrete mixture design was based on the proportions detailed in ASTM C1293.[26] High-alkali (0.99% Na_2O equivalent by mass of cement) general-use cement was used in the concrete mixture. The cement content of the mixture was 420 kg/m^3 (707.9 lb/yd^3). The chemical composition of cement used in this study is shown in Table 1. The alkali level of the concrete was boosted to 5.25 kg/m^3 (8.85 lb/yd^3) Na_2O equivalent by dissolving NaOH pellets in the mixing water. Spratt aggregate from Stittsville, ON, Canada, was used as the reactive coarse aggregate. Natural sand from Orillia, ON, Canada, was used as the nonreactive fine aggregate. No admixtures or supplementary cementitious materials were used. The water-cement ratio (w/c) of the mixture was 0.44. A similar but nonreactive mixture was used to cast control cylinder specimens. The nonreactive mixture was designed by substituting the siliceous limestone reactive coarse aggregate by nonreactive limestone coarse aggregate.

Casting of cube specimens

In total, 22 concrete cube specimens of 254 mm (10 in.) size were cast. Seven stress states were considered, from no-stress to triaxial stress, as shown in Table 2; all stresses are in compression. The stress level and precision level were chosen to be representative of typical prestressed concrete structures. As a reference, the prestressing compressive stress in concrete in biaxially prestressed containment structures of nuclear power plants ranged from 3.5 to 11 MPa (507.5 to 1595 psi).[20,27] For each stress state, three replicates were cast so that each set could also undergo destructive testing at three different ages

of accelerated curing. One specimen was cast as a reference to be destructively tested before stress application. The cube specimens were demolded after 1 day of casting.

Overall, the cube specimens were cast from nine batches of the same concrete mixture design. The average 28-day strength for the nine batches was 43.4 MPa (6295 psi) with a standard deviation of 2.9 MPa (419 psi). The average 28-day strength of the nonreactive mixtures was 49.4 MPa (7158 psi) with a standard deviation of 2.5 MPa (362 psi).

Loading and conditioning of specimens

The stress in the specimens was applied at an age of 52 to 56 days. The post-tensioning method of prestressing was chosen as the technique to apply and sustain the compressive stresses in the concrete specimens, and is detailed in Gautam and Panesar.[2] In any given direction, stress was applied by using four high-strength bolts with a diameter of either 12.7 or 19.0 mm (0.5 or 0.75 in.) tightened against a pair of bearing plates for each bolt. A neck was formed in each bolt by removing the threads from a 40 mm (1.6 in.) long section at the midlength. The neck was used for affixing a strain gauge to monitor the stress level in the bolt during stress application. (Stress level was monitored also during the conditioning of specimens, as detailed by Gautam.[28])

Corresponding to the four bolts, each loaded surface of a cube specimen consisted of four bearing plates. Two sizes of 19.0 mm (0.75 in.) thick plates were used for the two types of bolts—namely, 76 x 76 mm (3 x 3 in.) for the 12.7 mm (0.5 in.) bolt, and 102 x 102 mm (4 x 4 in.) for the 19.0 mm (0.75 in.) bolt. It should be noted that some non-uniformity in stress distribution prevailed in the specimens because stress was applied through bearing plates that partially covered the concrete surface.[28]

All specimens were cast with 12 stainless steel sheaths, four along each of the three mutually perpendicular directions. The bolts were inserted into the sheaths and hand-tightened first by carefully bringing the lead wire of the strain gauges underneath the bearing plates. Approximately 5 mm (0.2 in.) deep grooves were cut in the concrete surface to pass the lead wires located underneath the bearing plates.

Loading was performed using two wrenches. The stress application was controlled by observing the live strains in the bolts. The bolts had a yield strength exceeding 900 MPa (131 ksi). Reasonably constant stress state was maintained by stressing the bolts close to yielding. Any likely expansion due to ASR would yield the bolts and the stress level in the bolt would remain reasonably constant at the yield plateau for large strains exceeding 5000 microstrain (0.5% strain).

After the stress application, the cube specimens were stored on carts by maintaining an air space for moisture circulation on all the surfaces. Figure 1 shows a cart with the cube specimens. Any influence associated with the orientation of the specimens during storing/conditioning was minimized by changing the orientation of the specimens after each measurement.

From the day of demolding to the age of 6 months, the specimens were cured at room temperature (23 ± 3°C [73.4 ± 5.4°F]) with frequently watered wet burlap further covered with a plastic sheet. At the age of 6 months, the specimens

Fig. 1—Cube specimens with different stress states being stored on a cart.

were relocated to the acceleration chamber, maintained at 50 ± 0.5°C (122 ± 0.9°F) temperature and >95% relative humidity (RH). The specimens were periodically measured for expansion in the three directions, from 1 day to 18 months of casting. All the measurements on specimens during accelerated curing were taken only after removing the carts out from the chamber and acclimatizing the specimens at room temperature for approximately 24 hours.

Core testing

Cube specimens were core drilled by using a 75 mm (3 in.) diameter diamond drill bit cooled by water circulation. To avoid moisture loss, the drilled cores were wrapped with a cling-film. Each core was trimmed to discard a length of approximately 35 mm (1.4 in.) on either end. The remaining cylindrical piece was cut to a length of 150 mm (6 in.) and the ends were surface-ground. The core was affixed with concrete strain gauges (surface remained air-dried for approximately 2 hours during this process) and was tested for compressive strength as per ASTM C39[29] and static modulus of elasticity as per ASTM C469.[30]

Core drilling was performed at four stages of ASR (including one reference specimen and three replicate specimens) based on expansion measurements—namely, the first stage at 2 months of casting, the second stage at 3 months of accelerated curing (9 months after casting) when ASR was actively taking place, the third stage at 8 months of accelerated curing when the reaction was nearing to the completion, and the fourth stage at 12 months of accelerated curing when the expansion potential had exhausted. In each of the latter three stages, one cube specimen from each of the seven stress states was core-drilled after unbolting the prestressing bolts (thus releasing the stress). However, this test regime was modified in the case of the biaxial specimens. The coring of the biaxial specimens from the second stage was postponed until the third stage so that two identical cubes were avail-

Fig. 2—Dissection of no-stress cube specimen (254 mm [10 in.] size) along three mutually perpendicular planes (YZ, ZX, and XY) for DRI analysis and core-drilled along Z-axis.

Fig. 3—DRI slice from biaxial specimen along XY plane at 8 months of accelerated curing (grid size is 1 x 1 cm [0.4 x 0.4 in.]; length is 254 mm [10 in.]).

able at the third stage to simultaneously acquire in-place properties of one core along the X-direction and another core along the Z-direction. It was intended to minimize the time between unloading the cube specimens and core testing. The duration between unloading the cube specimens and coring was limited to 48 hours at most. Then, the cores were always tested the next day of coring. It should be noted that the specimens were measured for any change in length due to stress release during unbolting for coring. Expansion due to stress release was up to 0.025 mm (0.013%) along the stressed direction for the 9.6 MPa (1392 psi) stress that had caused 0.035 mm (0.018%) contraction during loading.

Damage rating index (DRI)

The portion of each cube specimen after core drilling was dissected for DRI analysis along the three mutually perpendicular planes, as shown in Fig. 2. The DRI method as outlined by Villeneuve et al.[31] was adopted in this study.

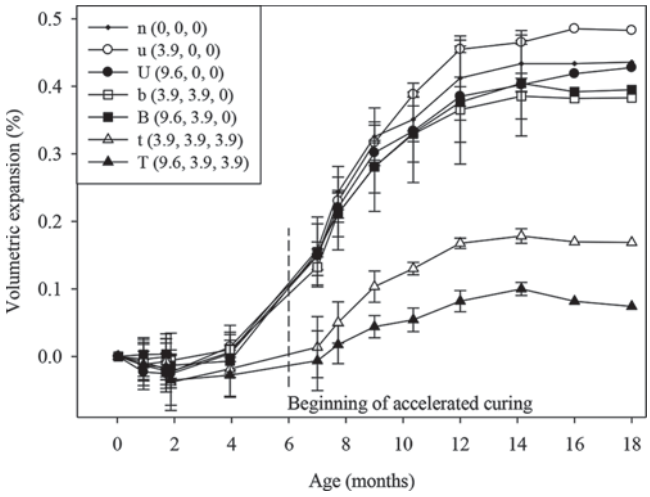

Fig. 4—Evolution of volumetric expansion of cube specimens with different stress states.

Table 3—Features counted in individual grid as per DRI method[31]

Petrographic features	Weighting factors
Closed/tight cracks in coarse aggregate particle	0.25
Opened cracks or network cracks in coarse aggregate particle	2
Cracks or network cracks with reaction product in coarse aggregate particle	2
Debonded coarse aggregate	3
Disaggregated/corroded aggregate particle	2
Cracks in cement paste	3
Cracks with reaction product in cement paste	3

Further reference was made to the guidelines published by Fournier et al.[32]

Slices from the cube specimens, with area ranging from 90 to 250 cm^2 (14 to 39 $in.^2$), were polished to a surface roughness of approximately 5 μm (0.2 mil) and were divided into 1 x 1 cm (0.4 x 0.4 in.) grids, as shown in Fig. 3. Each grid was observed in a stereo binocular microscope to count the number of seven petrographic features listed in Table 3. The number of counts were multiplied by the respective weighting factors and then summed. The sum was normalized to an area of 100 cm^2 (15.5 $in.^2$) to provide the DRI value for each plane. The DRI value for a cube specimen was obtained as the average for the three planes.

EXPERIMENTAL RESULTS AND DISCUSSION

Expansion

The evolution of volumetric expansion for the cube specimens over an 18-month duration is presented in Fig. 4. The rate of expansion with time was identical for the specimens except for the triaxially stressed specimens. However, the triaxially stressed specimens had a relatively lower rate of expansion until approximately 4.5 months of accelerated curing and a relatively higher rate of expansion between 4.5 and 8 months of accelerated curing (10.5 to 14 months of age). This indicated some delay in expansion contributed

by the triaxial confinement. However, for all stress states, the volumetric expansions of the cube specimens were practically constant between 8 and 12 months of accelerated curing, as shown in Fig. 4. Therefore, the expansions corresponding to the 12 months of accelerated curing were regarded as the ultimate expansions for the specimens in this study.

The ultimate longitudinal and volumetric expansions for the various stress states are presented in Fig. 5. The specimens underwent elastic shortening because of the stress application. This was indicated by the two sets of expansion measurements taken just before and after loading the specimens at an age of 8 weeks, as seen in Fig. 4. To exclude the elastic strain, the expansion due to ASR, as shown in Fig. 5, was considered with reference to the post-loading measurement. A slightly greater expansion was observed in the Z-direction than in the X- and Y-directions, particularly in the no-stress specimen. This is attributed to the anisotropy associated with casting direction.[33,34] A strong influence of stress state was observed on the ASR expansion, which was also reported previously.[2] Expansion in a given direction was reduced in the presence of stress applied in the same direction. Expansion was transferred from the stressed to the unstressed directions. Because ASR expansion was caused primarily by the fluid pressure of the reaction products, the pressure caused larger expansions in the free directions and lower expansions in the directions restrained by external compressive stresses. In general, a larger stress has a larger influence on the extent of reduction of the expansion as well as on the transfer of ASR expansion.

As shown in Fig. 4 and 5, the volumetric expansion due to ASR remained approximately constant irrespective of the stress state, with the exception of the triaxial stress state. Volumetric expansion for the uniaxially stressed specimens ("u" specimens) (3.9, 0, 0), was up to 18% larger compared to the no-stress specimens, which is attributed to the non-uniform stress distribution in the u (3.9, 0, 0) specimen.[28] The volumetric expansion was markedly reduced by 50 to 70% for the triaxially stressed specimens. These observations indicate that the volumetric expansion due to ASR is conserved as long as there is at least one unstressed direction. Accordingly, longitudinal expansion, measured by the concrete prism test for example, may be unconservative if regarded as the extent of expansion of concrete in a structure. For instance, a biaxially stressed concrete structure may show a relatively smaller expansion along the stressed directions; however, a relatively larger expansion—far greater than the linear expansion in an unstressed specimen—might occur in the out-of-plane direction.

Cracking

DRI along three planes for different stress states—The DRI values for the reference cube specimen tested at the age of 2 months were 74, 67, and 67, respectively, along YZ, ZX, and XY planes. Table 4 presents the DRI values for the cube specimens corresponding to the seven stress states at 3, 8, and 12 months of accelerated curing. DRI values increased with age for all the stress states, with an increase of 30 to 40% from 3 to 12 months of accelerated curing.

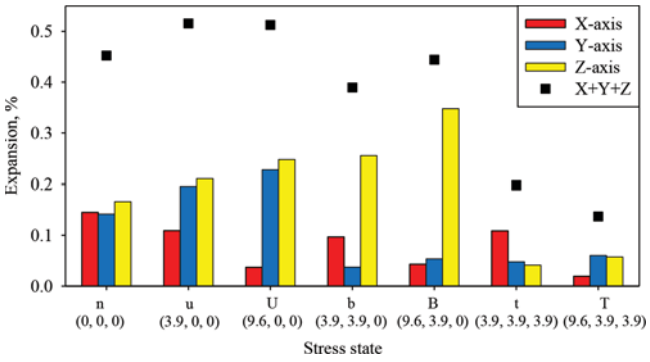

Fig. 5—Longitudinal and volumetric expansion (X + Y + Z) at 12 months of accelerated curing.

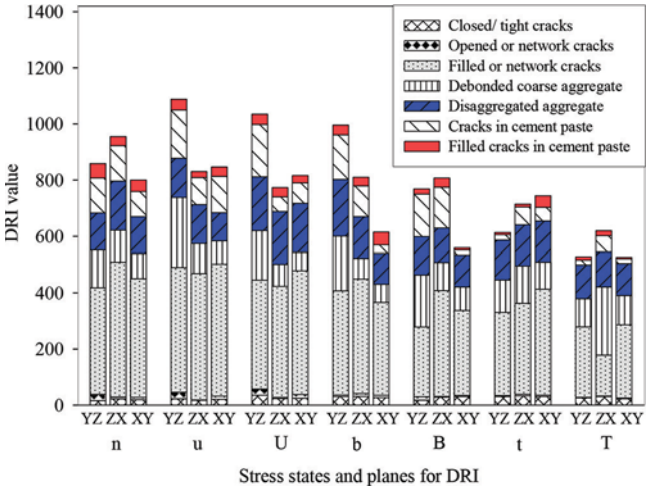

Fig. 6—Contributions of seven damage features to DRI along three planes of cube specimens at 12 months of accelerated curing.

Even though the extent of damage varied for different stress states, the reaction was not prevented by the stresses. As shown in Table 4, the DRI values for the triaxially stressed specimens t (3.9, 3.9, 3.9) and T (9.6, 3.9, 3.9), respectively, are approximately 78% and 64% of the DRI value for the no-stress specimen n (0, 0, 0) at the same age. Figure 6 shows the contributions of the seven damage features to the DRI values of the specimens for all the stress states at 12 months of accelerated curing. All the damage features of DRI were abundantly observed in the specimens of all the stress states.

Figure 6 shows the variation of DRI values along the three mutually perpendicular planes YZ, ZX, and XY. The DRI value for a given plane was sensitive to the stress state in the plane. Stress prevented crack opening along the direction of stress, which was reflected in the DRI results. A crack opening along a particular direction was generally in agreement with the axial expansion in that direction. Accordingly, in a cube specimen, the DRI value was generally the greatest in the plane that contained directions with the largest expansions, and vice versa. Hence, the DRI value in the YZ plane of the uniaxially stressed specimens was considerably larger than the DRI values in the ZX and XY planes. For the biaxially stressed specimens, the DRI value in the XY plane was considerably smaller than in the YZ and ZX planes. While

Table 4—DRI results for cube specimens

Stress state	Plane for DRI analysis	3 months of accelerated curing			8 months of accelerated curing			12 months of accelerated curing		
		DRI value (plane)	Average DRI value (specimen)	Ratio with n (0, 0, 0)	DRI value (plane)	Average DRI value (specimen)	Ratio with n (0, 0, 0)	DRI value (plane)	Average DRI value (specimen)	Ratio with n (0, 0, 0)
n (0, 0, 0)	YZ	677	630	1.00	799	843	1.00	859	871	1.00
	ZX	604			849			955		
	XY	608			880			800		
u (3.9, 0, 0)	YZ	812	696	1.10	882	775	0.92	1088	922	1.06
	ZX	572			723			830		
	XY	704			721			847		
U (9.6, 0, 0)	YZ	820	686	1.09	874	790	0.94	1035	875	1.00
	ZX	575			761			773		
	XY	664			734			816		
b (3.9, 3.9, 0)	YZ	—	—	—	711	673	0.80	996	807	0.93
	ZX	—			783			810		
	XY	—			523			615		
B (9.6, 3.9, 0)	YZ	—	—	—	731	700	0.83	768	712	0.82
	ZX	—			833			807		
	XY	—			536			559		
t (3.9, 3.9, 3.9)	YZ	504	493	0.78	476	648	0.77	614	691	0.79
	ZX	493			674			714		
	XY	481			794			744		
T (9.6, 3.9, 3.9)	YZ	526	407	0.65	671	534	0.63	528	558	0.64
	ZX	327			451			620		
	XY	369			480			526		

the YZ and ZX planes had one direction (Z) free to expand, the XY plane had stresses in both X- and Y- directions. Thus, XY was the preferential plane for the smallest damage (cracking) in the biaxially stressed specimens.

Stress in ASR-affected concrete was effective to reduce the cracking of the mortar matrix, referred to as the paste cracking in the DRI method. As shown in Fig. 6, the contribution of paste cracks (both the "cracks in cement paste" and the "filled cracks in cement paste") to the DRI value was markedly small in the XY plane of the biaxially stressed b (3.9, 3.9, 0) and B (9.6, 3.9, 0) specimens and in all three planes of the triaxially stressed t (3.9, 3.9, 3.9) and T (9.6, 3.9, 3.9) specimens. While the combined contribution of the "cracks in cement paste" and the "filled cracks in cement paste" was approximately 15 to 20% for the no-stress, uniaxial, and biaxial stress conditions, its contribution for the triaxial stress condition was less than 15% for t (3.9, 3.9, 3.9) and less than 8% for T (9.6, 3.9, 3.9) specimens. Thus, while the stresses are unlikely to prevent the reaction, they can still be effective in reducing the ASR damage of concrete.

Expansion-DRI relationship—In general, for all stress states, the DRI value of the cube specimen was proportional to the volumetric expansion, as shown in Fig. 7. However, a DRI value of approximately 70 had been observed at the age of 2 months even before ASR expansion had occurred. The DRI versus volumetric expansion data fit well to a power

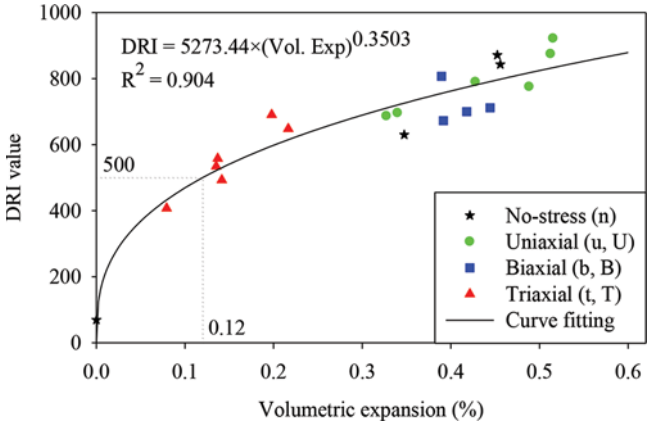

Fig. 7—Average DRI versus volumetric expansion for all cube specimens with different stress states and at different test ages, and a curve fitting.

equation with R^2 = 0.904. By taking into account the DRI value that was observed even before the ASR expansion had occurred, the curve indicates that a significant level of microcracking can occur inside concrete before any macroscopic expansion is evident.

Axial (longitudinal) expansion of 0.04% is often accepted as a safe expansion[26] that can be accommodated by concrete without undergoing visible surface cracking. However, Fig. 7 shows that a DRI value of 500 is possible corresponding to

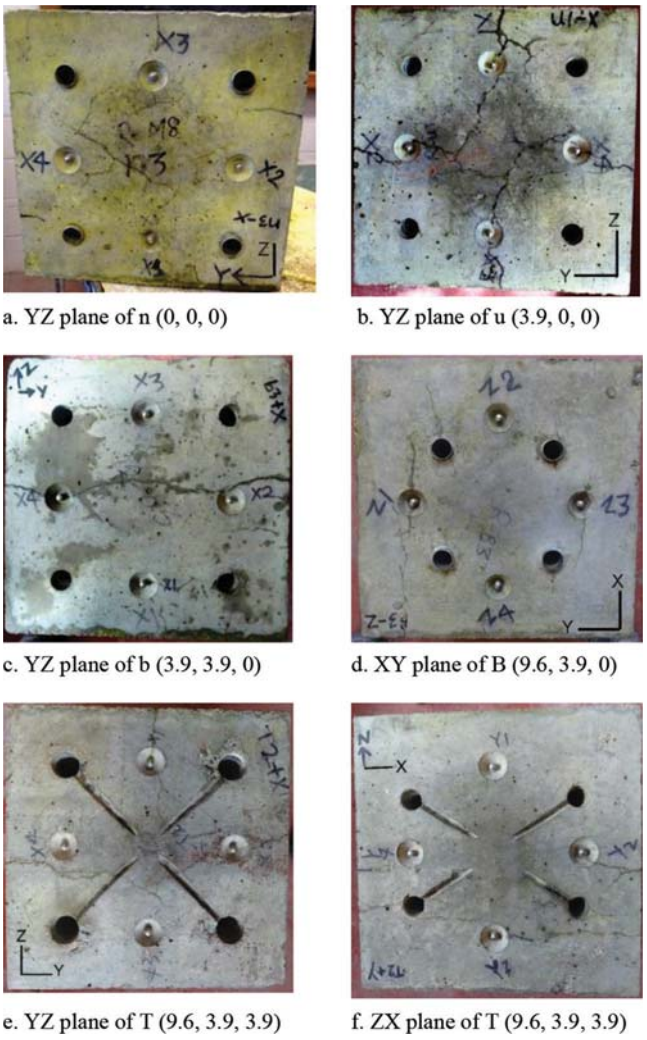

a. YZ plane of n (0, 0, 0)
b. YZ plane of u (3.9, 0, 0)
c. YZ plane of b (3.9, 3.9, 0)
d. XY plane of B (9.6, 3.9, 0)
e. YZ plane of T (9.6, 3.9, 3.9)
f. ZX plane of T (9.6, 3.9, 3.9)

Fig. 8—Cracks on some cube specimen (254 mm [10 in.] size) surfaces at 12 months of accelerated curing.

a volumetric expansion of 0.12%, which is equivalent to a uniform linear expansion of 0.04% in all three directions. Because ASR expansion can transfer from one direction to another, depending on the stress state, the interpretation of ASR expansion and damage should consider the consequences in all three directions.

Surface cracking—Figure 8 shows six photographs of the selected cube surfaces exhibiting surface cracking at 12 months of accelerated curing. Even though the cracks were generally fine with a maximum width of approximately 0.5 mm (0.02 in.), the photographs reveal the influence of stress states on surface cracking. Figure 8(a) shows that the no-stress n (0, 0, 0) specimens exhibited a map cracking pattern, a characteristic of ASR in unreinforced or slightly reinforced concrete structures. Figure 8(b) shows cracking along the centrelines of the cube surface of the uniaxially stressed u (3.9, 0, 0) specimen. This was the characteristic cracking pattern in the YZ plane of the uniaxially stressed specimens. Because stress was along the X-direction, larger expansion was observed in the Y- and Z-directions. Accordingly, the cracks were clearly oriented such that the crack openings were in the Y- and Z-directions.

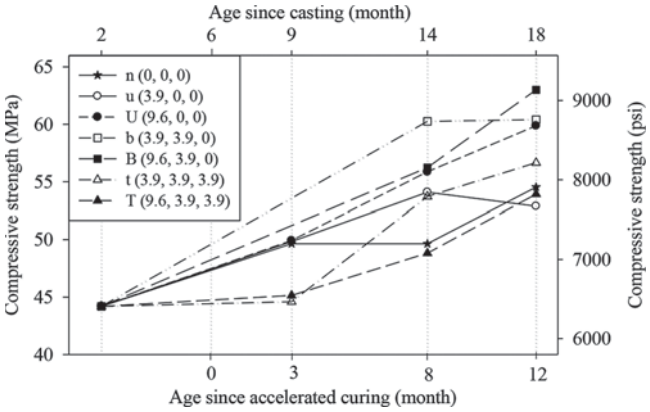

Fig. 9—Compressive strength of cores taken along X-direction from cube specimens.

A similar effect of stress in aligning the cracks was further exhibited by the cracking patterns in the biaxially stressed specimens. Figure 8(c) shows a central crack covering the entire surface in the YZ plane of the b (3.9, 3.9, 0) specimen. The crack occurred along the Y-direction such that the crack opening was directed along the unrestrained Z-direction. Figure 8(d) shows the photograph of the XY plane of the biaxially stressed B (9.6, 3.9, 0) specimen. Relatively finer cracks were aligned along the X-direction. Even though both X- and Y-directions were restrained, the stress in the Y-direction was smaller than that in the X-direction. Thus, the cracks were aligned along the X-direction.

The effect of stress was exhibited by the surface cracks in the triaxially stressed specimens as well. Figure 8(e) shows the photograph of the YZ plane of the triaxially loaded T (9.6, 3.9, 3.9) specimen. Having similar stresses in the Y- and Z-directions, an approximately identical crack opening was observed along the Y- and Z-directions. Figure 8(f) shows the ZX plane of the triaxially loaded T (9.6, 3.9, 3.9) specimen. Because the stress level in the Z-direction was smaller than in the X-direction, the cracks opened along the Z-direction.

Effect of ASR on mechanical properties

Core test results—The compressive strength results of the cores at 2 months of casting and at 3, 8, and 12 months of accelerated curing are presented in Fig. 9. Each data point in the figure represents the result of one core sample. The figure compares the test results along the X-direction (the direction of maximum stress) for all the specimens. Stress along the X-direction appears to improve the compressive strength, even though a clear relationship of compressive strength with stress state could not be observed. Compressive strength of cores generally increased with age for all the stress states and was unable to reflect the damage due to ASR. The evolution of compressive strength is further discussed in the next section in relation to the cylinder test results.

The static modulus of elasticity of the cores at 2 months of casting and at 3, 8, and 12 months of accelerated curing is presented in Fig. 10. The figure compares the test results along the X-direction of the specimens. After 8 months of accelerated curing, the modulus of elasticity for the no-stress spec-

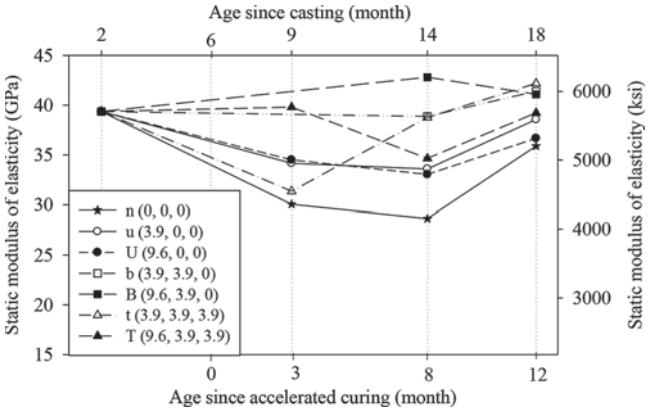

Fig. 10—Static modulus of elasticity of cores taken along X-direction from cube specimens.

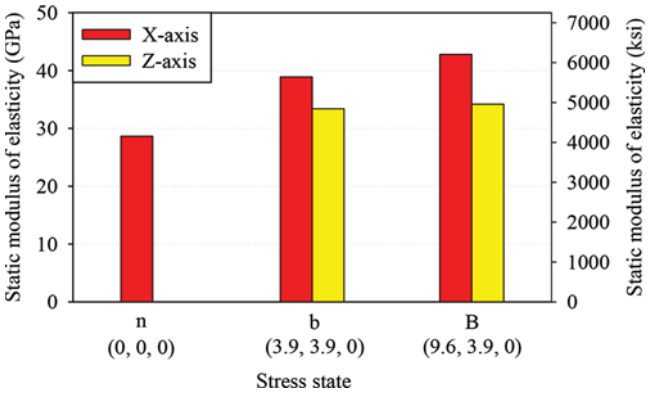

Fig. 11—Static modulus of elasticity along stressed and unstressed directions in biaxially stressed specimens.

imen dropped by a maximum of 27% of the value at 2 months of casting. However, stress along the X-direction alleviated the loss in the modulus of elasticity. The maximum degradation was limited to 15% when a stress of 3.9 MPa (566 psi) was present along the X-direction. Biaxial and triaxial stresses further alleviated the loss in the modulus of elasticity. These observations suggest that stress state could be beneficial for many concrete structures in resisting any likely loss in the modulus of elasticity due to ASR. The evolution of static modulus of elasticity is further discussed in the next section in relation to the cylinder test results.

Figure 11 compares the modulus of elasticty in the biaxially stressed specimens along the direction of maximum stress (X) and along the direction of no-stress (Z) tested after 8 months of acccelerated curing. The static modulus of elasticity was larger in the X-direction than in the Z-direction by 16% and 25%, respectively, for the b (3.9, 3.9, 0) and B (9.6, 3.9, 0) specimens. Although slight effect of casting direction might have occurred, these results primarily indicate that the crack closure effect (for the cores in the Z-direction) contributes to reducing the static modulus of elasticity. Stress turned the ASR-affected concrete into an orthotropic material.

Cylinder test results—Nonreactive (control) cylinders and reactive cylinders, cast from the same concrete batches as of the cube specimens, were tested for compressive strength, modulus of elasticity, and splitting tensile strength. The results are presented in Fig. 12, 13, and 14, respectively.

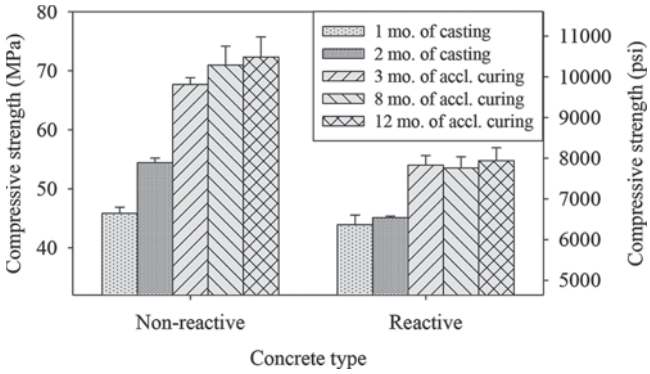

Fig. 12—Compressive strength of nonreactive and reactive cylinders.

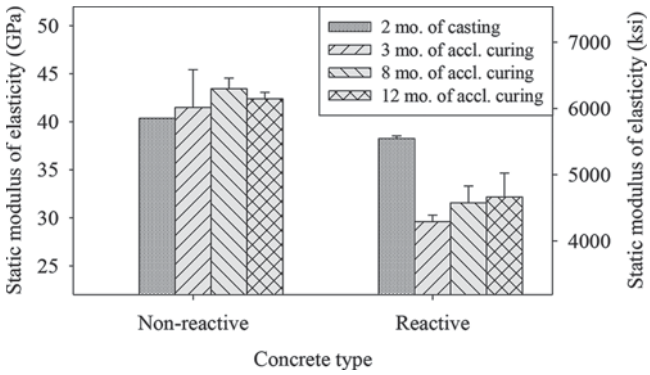

Fig. 13—Static modulus of elasticity of nonreactive and reactive cylinders.

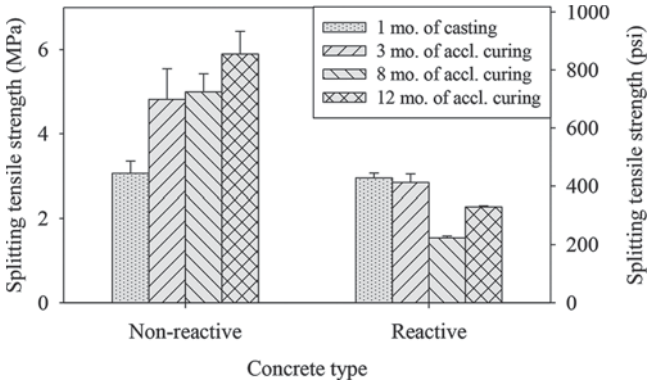

Fig. 14—Splitting tensile strength of nonreactive and reactive cylinders.

Compressive strength increased for both the reactive and nonreactive cylinders from 1 month of casting to 12 months of accelerated curing (18 months of casting). The increase was approximately 24% for reactive and 58% for the nonreactive cylinders. The relatively smaller increase in the compressive strength of the reactive specimens compared to the nonreactive specimens reflects the combined effects of ASR and hydration reaction. Curing at 50 ± 0.5°C (122 ± 0.9°F) and >95% RH promoted the continued hydration of concrete, which offset the damage caused by ASR.

With accelerated curing, the modulus of elasticity of the nonreactive concrete increased by 5 to 8% compared to the value at 2 months of casting. However, a loss was observed in the modulus of elasticity of the reactive concrete. The

maximum loss of 23% (compared to the value at 2 months of casting) was observed after having 3 months of accelerated curing. The level of degradation was comparable to that from the core test (27%).

While the splitting tensile strength for the nonreactive specimens increased by 93%, it was degraded by a maximum of 53% for the reactive specimens, before a partial recovery was observed.

SUMMARY AND CONCLUSIONS

This study investigated the expansion, cracking, and degradation of the mechanical properties of ASR-affected concrete subjected to seven different compressive stress states—namely, no-stress and two variations each of uniaxial, biaxial, and triaxial stresses. The following are the key findings:

1. ASR axial expansion was highly sensitive to the stress state of concrete and behaved as a directional property. ASR axial expansion was reduced due to stress and transferred to a no-stress direction. ASR attempts to conserve the volumetric expansion in concrete as long as one unstressed direction is available.

2. The expansion transfer mechanism was confirmed by the DRI results. The comparison of DRI values along different planes demonstrated that even the biaxial confinement was not adequate to suppress ASR damage. However, triaxial specimens showed markedly smaller DRI values compared to the other stress conditions, suggesting that the triaxial confinement can reduce ASR damage. Even though the triaxial confinement did not prevent the reaction, the triaxial confinement was effective to largely reduce cracking, particularly the mortar matrix cracking.

3. The stress state influenced the opening of cracks. Cracks were opened preferentially along the unstressed direction or the direction with a relatively smaller compressive stress.

4. Similar to the ASR axial expansion, the cracking of concrete and the change in mechanical properties showed a directional behavior with the stress state. The loss in static modulus of elasticity was the greatest for the no-stress specimens compared to the stressed specimens. The modulus of elasticity was observed to be anisotropic as a direct result of the directional stress state.

5. Triaxial compressive stress in ASR concrete contributed to having reduced volumetric expansion, lower DRI value, less cracking, and less overall degradation of the mechanical properties.

This study integrates the understanding of the three main effects of ASR—expansion, cracking, and degradation of mechanical properties of concrete in the context of concrete structures. The findings from this study will be useful in the analysis of reinforced and multiaxially stressed concrete structures—in particular, suggesting the necessity of treating ASR-affected concrete as an orthotropic material. This is anticipated to increase the accuracy of numerical analysis. Similar studies with various types of reactive aggregates and various mixture designs will improve the understanding of the consequences of ASR in the concrete structures.

This study highlights that consideration of the stress state of concrete is important in planning field investigation of ASR-affected structures, particularly to ascertain the direction of expansion measurement and coring, and in interpreting the field investigation results. In the assessment of ASR-affected structures, monitoring of ASR expansion may underestimate the severity of ASR progression if the direction chosen for the monitoring happens to be the highly stressed direction, and vice versa. Similarly, results from core testing should be interpreted for ASR damage with reference to the direction of coring relative to the stress state of concrete. Stress state can markedly affect the ASR performance of concrete by affecting ASR expansion, influencing opening and orientation of ASR cracks, and associating directional effect on the mechanical properties of concrete. An accurate diagnosis and prognosis of an ASR-affected structure will be possible only when stress state is considered.

AUTHOR BIOS

ACI member **Bishnu Prasad Gautam** *is Managing Director at Sarthak Concrete P. Ltd., Kathmandu, Nepal. He received his PhD from the University of Toronto, Toronto, ON, Canada in 2016. He received his ME from the University of Tokyo, Tokyo, Japan, and his BE from Tribhuvan University, Kirtipur, Nepal. He was the winner of the Ontario Chapter – ACI's 2012 Nick Bada Ontario Chapter Graduate Scholarship. His research interests include the materials and mechanics aspects of concrete structures, and the application of precast and prestressed concrete.*

ACI member **Daman K. Panesar** *is an Associate Professor in the Department of Civil Engineering at the University of Toronto. Her research interests include advancing concrete materials, low-carbon materials, material characterization, and durability performance of aging infrastructure.*

Shamim A. Sheikh, *FACI, is a Professor of civil engineering at the University of Toronto. He is a past Chair and member of Joint ACI-ASCE Committee 441, Reinforced Concrete Columns, and a member of ACI Committee 374, Performance-Based Design of Concrete Structures. He received the ACI Chester Paul Seiss Award for Excellence in Structural Research in 1999. His research interests include earthquake resistance and design of concrete structures, concrete confinement, and the use of fiber-reinforced polymer for sustainable concrete structures.*

Frank J. Vecchio, *FACI, is a Professor in the Department of Civil Engineering at the University of Toronto. He is a member of Joint ACI-ASCE Committees 441, Reinforced Concrete Columns, and 447, Finite Element Analysis of Reinforced Concrete Structures. He received the 1998 ACI Structural Research Award, the 1999 ACI Structural Engineer Award, and the 2011 ACI Wason Medal for Most Meritorious Paper. His research interests include advanced constitutive modeling and analysis of reinforced concrete, and assessment and response of structures under extreme loads.*

ACKNOWLEDGMENTS

This research was conducted with the funding through a contract with Canadian Nuclear Safety Commission (CNSC). However, the contents of this paper does not represent the technical position of the CNSC. The authors acknowledge the support from the Ministry of Transportation Ontario, Canada, for providing the reactive Spratt aggregate; Lafarge Canada Inc. for Orillia sand; and Holcim Canada Inc. for cement.

REFERENCES

1. Doran, D.; Douglas, J.; and Pratley, R., *Refurbishment and Repair in Construction*, Whittles Publishing, Dunbeath, UK, 2009, 314 pp.

2. Gautam, B. P., and Panesar, D. K., "A New Method of Applying Long-Term Multiaxial Stresses in Concrete Specimens Undergoing ASR, and Their Triaxial Expansions," *Materials and Structures*, V. 49, No. 9, 2016, pp. 3495-3508. doi: 10.1617/s11527-015-0734-z

3. Berra, M.; Faggiani, G.; Mangialardi, T.; and Paolini, A. E., "Influence of Stress Restraint on the Expansive Behaviour of Concrete Affected by Alkali-Silica Reaction," *Cement and Concrete Research*, V. 40, No. 9, 2010, pp. 1403-1409. doi: 10.1016/j.cemconres.2010.05.002

4. Multon, S., and Toutlemonde, F., "Effect of Applied Stresses on Alkali-Silica Reaction-Induced Expansions," *Cement and Concrete Research*, V. 36, No. 5, 2006, pp. 912-920. doi: 10.1016/j.cemconres.2005.11.012

5. Kagimoto, H.; Yasuda, Y.; and Kawamura, M., "ASR Expansion, Expansive Pressure and Cracking in Concrete Prisms under Various

Degrees of Restraint," *Cement and Concrete Research*, V. 59, No. 05, 2014, pp. 1-15. doi: 10.1016/j.cemconres.2014.01.018

6. Giannini, E. R.; Bentivegna, A. F.; and Folliard, K. J., "Strain Gradients in Concrete Affected by Alkali-Silica Reaction: A Laboratory Simulation," *Advances in Civil Engineering Materials*, V. 3, No. 1, 2014, pp. 388-403. doi: 10.1520/ACEM20130114

7. Thomas, M. D. A.; Folliard, K. J.; Fournier, B.; Rivard, P.; and Drimalas, T., "Methods for Evaluating and Treating ASR-Affected Structures: Results of Field Application and Demonstration Projects; Vol II: Details of Field Applications and Analysis," Federal Highway Administration, Washington, DC, 2013, 320 pp.

8. Thomas, M. D. A.; Fournier, B.; Folliard, K. J.; and Resendez, Y. A., *Alkali-Silica Reactivity Field Identification Handbook*, Federal Highway Administration, Washington, DC, 2011, 69 pp.

9. Rivard, P.; Fournier, B.; and Ballivy, G., "The Damage Rating Index Method for ASR Affected Concrete—A Critical Review of Petrographic Features of Deterioration and Evaluation Criteria," *Cement, Concrete and Aggregates*, V. 24, No. 2, 2002, pp. 1-11.

10. Rivard, P., and Ballivy, G., "Assessment of the Expansion Related to Alkali-Silica Reaction by the Damage Rating Index Method," *Construction and Building Materials*, V. 19, No. 2, 2005, pp. 83-90. doi: 10.1016/j.conbuildmat.2004.06.001

11. Sanchez, L. F. M.; Fournier, B.; Jolin, M.; and Duchesne, J., "Reliable Quantification of AAR Damage through Assessment of the Damage Rating Index (DRI)," *Cement and Concrete Research*, V. 67, 2015, pp. 74-92. doi: 10.1016/j.cemconres.2014.08.002

12. Grattan-Bellew, P. E., "Laboratory Evaluation of Alkali-Silica Reaction in Concrete from Saunders Generating Station," *ACI Materials Journal*, V. 92, No. 2, Mar.-Apr. 1995, pp. 126-133.

13. Swamy, R. N., and Al-Asali, M. M., "Engineering Properties of Concrete Affected by Alkali-Silica Reaction," *ACI Materials Journal*, V. 85, No. 5, Sept.-Oct. 1988, pp. 367-374.

14. Marzouk, H., and Langdon, S., "The Effect of Alkali-Aggregate Reactivity on the Mechanical Properties of High and Normal Strength Concrete," *Cement and Concrete Composites*, V. 25, No. 4-5, 2003, pp. 549-556. doi: 10.1016/S0958-9465(02)00094-X

15. Ahmed, T.; Burley, E.; Rigden, S.; and Abu-Tair, A. I., "The Effect of Alkali Reactivity on the Mechanical Properties of Concrete," *Construction and Building Materials*, V. 17, No. 2, 2003, pp. 123-144. doi: 10.1016/S0950-0618(02)00009-0

16. Giaccio, G.; Zerbino, R.; Ponce, J. M.; and Batic, O. R., "Mechanical Behavior of Concretes Damaged by Alkali-Silica Reaction," *Cement and Concrete Research*, V. 38, No. 7, 2008, pp. 993-1004. doi: 10.1016/j.cemconres.2008.02.009

17. Pantazopoulou, S. J., and Thomas, M. D. A., "Modeling Stress-Strain Behavior of Concrete Damaged by Alkali-Aggregate Reaction (AAR)," *ACI Structural Journal*, V. 96, No. 5, Sept.-Oct. 1999, pp. 790-802.

18. Giaccio, G.; Torrijos, M. C.; Tobes, J. M.; Batic, O. R.; and Zerbino, R., "Development of Alkali-Silica Reaction under Compressive Loading and its Effects on Concrete Behavior," *ACI Materials Journal*, V. 106, No. 3, May-June 2009, pp. 223-230.

19. Barbosa, R. A., and Hansen, K. K., "The Influence of Alkali-Silica Reaction and Crack Orientation on the Mechanical Properties of Concrete," *The 10th fib International PhD Symposium in Civil Engineering*, Quebec, QC, Canada, July 2014, pp. 111-116.

20. Tcherner, J., and Aziz, T.S., "Effects of AAR on Seismic Assessment of Nuclear Power Plants for Life Extensions," *SMiRT 20*, Espoo, Finland, Aug. 2009, 8 pp.

21. Sanchez, L. F. M.; Fournier, B.; Jolin, M.; and Bastien, J., "Evaluation of the Stiffness Damage Test (SDT) as a Tool for Assessing Damage in Concrete Due to ASR: Test Loading and Output Responses for Concretes Incorporating Fine or Coarse Reactive Aggregates," *Cement and Concrete Research*, V. 56, No. 2, 2014, pp. 213-229. doi: 10.1016/j.cemconres.2013.11.003

22. Giannini, E. R., and Folliard, K. J., "Stiffness Damage and Mechanical Testing of Core Specimens for the Evaluation of Structures Affected by ASR," *Proceedings of the 14th International Conference on Alkali Aggregate Reaction*, Austin, TX, May 2012, 10 pp.

23. Chrisp, T. M.; Waldron, P.; and Wood, J. G. M., "Development of a Non-Destructive Test to Quantify Damage in Deteriorated Concrete," *Magazine of Concrete Research*, V. 45, No. 165, 1993, pp. 247-256. doi: 10.1680/macr.1993.45.165.247

24. Jones, A. E. K., and Clark, L. A., "The Effects of ASR on the Properties of Concrete and the Implications for Assessment," *Engineering Structures*, V. 20, No. 9, 1998, pp. 785-791. doi: 10.1016/S0141-0296(97)00125-9

25. ACI Committee 214, "Guide for Obtaining Cores and Interpreting Compressive Strength Results (ACI 214.4R-10)," American Concrete Institute, Farmington Hills, MI, 2010, 17 pp.

26. ASTM C1293-08, "Standard Test Method for Determination of Length Change of Concrete due to Alkali-Silica Reaction," ASTM International, West Conshohocken, PA, 2008, 7 pp.

27. Anderson, P., "Thirty Years of Measured Prestress at Swedish Nuclear Reactor Containments," *Nuclear Engineering and Design*, V. 235, No. 21, 2005, pp. 2323-2336. doi: 10.1016/j.nucengdes.2005.04.002

28. Gautam, B. P., "Multiaxially Loaded Concrete Undergoing Alkali-Silica Reaction (ASR)," PhD thesis, University of Toronto, Toronto, ON, Canada, 2016, 187 pp.

29. ASTM C39-10, "Standard Test Method for Compressive Strength of Cylindrical Concrete Specimens," ASTM International, West Conshohocken, PA, 2010, 7 pp.

30. ASTM C469-10, "Standard Test Method for Static Modulus of Elasticity and Poisson's Ratio of Concrete in Compression," ASTM International, West Conshohocken, PA, 2010, 5 pp.

31. Villeneuve, V.; Fournier, B.; and Duchesne, J., "Determination of the Damage in Concrete Affected by ASR—The Damage Rating Index (DRI),"*Proceedings of the 14th International Conference on Alkali-Aggregate Reaction in Concrete*, Austin, TX, May 2012, 10 pp.

32. Fournier, B.; Fecteau, P. L.; Villeneuve, V.; Tremblay, S.; and Sanchez, L. F. M., "Description of Petrographic Features of Damage in Concrete Used in the Determination of the Damage Rating Index (DRI)," Laval University, Quebec, QC, Canada, 2015, 59 pp.

33. Smaoui, N.; Berube, M.; Fournier, B.; and Bissonnette, B., "Influence of Specimen Geometry, Orientation of Casting Plane, and Mode of Concrete Consolidation on Expansion due to ASR," *Cement, Concrete and Aggregates*, V. 26, No. 2, 2004, pp. 58-70. doi: 10.1520/CCA11927

34. Multon, S.; Seignol, J. F.; and Toutlemonde, F., "Structural Behavior of Concrete Beams Affected by Alkali-Silica Reaction," *ACI Materials Journal*, V. 102, No. 2, Mar.-Apr. 2005, pp. 67-76.